Vol 12 No 6, June 2003
1009-1963/2003/12(06)/0610-05

Chinese Physics

© 2003 Chin. Phys. Soc.
and IOP Publishing Ltd

Cell image recognition with radial harmonic Fourier moments*

Ren Hai-Ping(任海萍)[a)†], Ping Zi-Liang(平子良)[b)], Bo Wu-Ri-Gen(博午日亘)[c)]
Sheng Yun-Long(盛云龙)[d)], Chen Sheng-Zu(陈盛祖)[a)], and Wu Wen-Kai(吴文凯)[a)]

[a)] *Department of Nuclear Medicine, Cancer Hospital, Chinese Academy of Medical Sciences, Peking Union Medical College, Beijing* 100021, *China*
[b)] *Department of Physics, Inner Mongolia Normal University, Huhhot* 010022, *China*
[c)] *Mathematics Institute, Peking University, Beijing* 100871, *China*
[d)] *Department of Physics, Laval University, Quebec, GIK 7P4, Canada*

(Received 18 November 2002; revised manuscript received 18 February 2003)

Various types of moments have been utilized to recognize image patterns in a number of applications. Multi-distortion invariant—radial harmonic Fourier moments were investigated in the recognition of cell smear images. Image recognition experiments showed that radial harmonic Fourier moments are not only highly concentrated image features but also have a good property of antidistortion and antinoise. They may be used in fast and accurate automatic cell recognition.

Keywords: cell recognition, moment invariant
PACC: 4230, 4230K, 4230S

1. Introduction

Moment is a highly concentrated image feature that has the invariant properties of moment function in multi-distortion of an image such as translation, scaling, rotation, and changing intensity. Therefore, it has been extensively employed as the invariant global features of an image in pattern recognition, image classification, target identification, and scene analysis.[1]

Hu[2] first introduced geometric moments invariant in 1961, from which image was hard to be recovered. Teague[3] introduced Zernike moments based on the theory of orthogonal polynomials. Other orthogonal moments are rotational moments,[4] complex moments,[5] and Legendre moments.[6] Teh and Chin[6] evaluated various types of moments and found that Zernike moments outperformed the others in terms of overall performances for image description and robustness to noise. Sheng and Shen[7] proposed orthogonal Fourier–Mellin moments (OFMMs) in 1994, which have better properties than Zernike moments for describing an image. In 2002, Ping *et al*[8] introduced Chebyshev–Fourier moments (CHFMs) which have nearly the same performance as OFMMs. We also suggested to choose a triangular function as the radial function and proposed new moments named radial harmonic Fourier moments (RHFMs).[9] Compared with CHFMs, RHFMs have a superior performance near the origin and better description ability for small images in terms of image reconstruction errors and noise sensitivity.

Cytological examination is indispensable for clinical diagnosis, therapy and research. It is extensively used for diagnosis of haemal system diseases, contagious diseases and tumours by samples of blood, cerebrospinal fluid and pleural effusion. However, the examination is nearly completely done by experienced experts, which is time consuming and hard sledding, thus not suitable for disease screening. Automatic, fast and accurate cell image recognition is needed to be realized urgently.

So, we use some cell slice images to investigate the application properties of RHFMs. In this paper, various cell images are described with RHFMs as the feature and then the multi-distortion invariant pattern

*Project supported by the National Natural Science Foundation (Grant No 60262001) and by the Inner Mongolia Natural Science Foundation, China (Grant No 201301).
†Corresponding author. E-mail: haipingren@163.com, Tel: +86-10-67781331 ext 8599(O), Fax: +86-10-67723793

recognition experiment is performed. Results show that as good image features, RHFMs are suitable for fast and accurate cell recognition, and thus have great potential for further applications.

2. Radial harmonic Fourier moments

2.1. Definition

A function set $P_{nm}(r,\theta)$ defined in a polar coordinate system (r,θ) contains a radial function $T_n(r)$ and a Fourier factor in the angle direction $\exp(\mathrm{j}m\theta)$:

$$P_{nm}(r,\theta) = T_n(r)\exp(\mathrm{j}\,m\theta), \tag{1}$$

where

$$T_n(r) = \begin{cases} \dfrac{1}{\sqrt{r}}, & \text{if} \quad n=0; \\ \sqrt{\dfrac{2}{r}}\sin[(n+1)\pi r], & \text{if} \quad n=\text{odd}; \\ \sqrt{\dfrac{2}{r}}\cos(n\pi r), & \text{if} \quad n=\text{even}. \end{cases} \tag{2}$$

The set of $P_{nm}(r,\theta)$ is orthogonal over the range $0 \le r \le 1$,

$$\int_0^{2\pi}\int_0^1 P_{nm}(r,\theta)P_{kl}(r,\theta)r\,\mathrm{d}r\,\mathrm{d}\theta = \delta_{nmkl}, \tag{3}$$

where δ_{nmkl} is the Kronecker symbol, and r=1 is the maximum size of the objects that can be encountered in a particular application. The image $f(r,\theta)$ can be decomposed with the set of $P_{nm}(r,\theta)$ as

$$f(r,\theta) = \sum_{n=0}^{\infty}\sum_{m=-\infty}^{+\infty} \Phi_{nm}T_n(r)\exp(\mathrm{j}\,m\theta), \tag{4}$$

where

$$\Phi_{nm} = \int_0^{2\pi}\int_0^1 f(r,\theta)T_n(r)\exp(-\mathrm{j}\,m\theta)r\,\mathrm{d}r\,\mathrm{d}\theta. \tag{5}$$

We define Φ_{nm} as RHFMs.

2.2. Normalization and invariance

RHFMs are not invariant themselves, however, they can be normalized into invariant for shifting, scaling, rotation and intensity distortion of an image.[5] Firstly, we use the first-order geometrical moments to determine the centre of the image, which is taken as the origin of the coordinate system. All the moments calculated in this coordinate system are shift invariant. Secondly, since the angle function is a Fourier factor, a rotation of the image by an angle φ will result in a phase factor $\mathrm{e}^{\mathrm{j}\,m\varphi}$ for all orders of Φ'_{nm}. The modulus of RHFMs, $|\Phi'_{nm}|$, are rotational invariant. Finally, lower-order Fourier–Mellin transfer $\dfrac{M^i_{10}}{M^i_{00}}$[4] is computed for every distorted image in the training set. We use the following formulae (6) and (7) to calculate k_i and g_i respectively for each image with the ratio $\dfrac{M_{10}}{M_{00}}$ being a constant and slightly smaller than the minimum $\dfrac{M^i_{10}}{M^i_{00}}$ of all the images in the training set to ensure that the normalized images remain inside the unit circle.

$$k_i = \left(\frac{M^i_{10}}{M^i_{00}}\right) \Big/ \left(\frac{M_{10}}{M_{00}}\right), \tag{6}$$

$$g_i = \left[\left(\frac{M_{10}}{M_{00}}\right) \Big/ \left(\frac{M^i_{10}}{M^i_{00}}\right)\right]^2 \cdot \frac{M'_{00}}{M_{00}}. \tag{7}$$

Φ_{nm} is then calculated by formulae (8) and (9) for all images of the training set, which is scaling and intensity distortion invariant.

$$\phi^i_{nm} = \int_0^{2\pi}\int_0^{k_i} g_i f(r/k_i,\theta)T_n(r/k_i)\mathrm{e}^{-\mathrm{j}\,m\theta}r\,\mathrm{d}\,r\,\mathrm{d}\,\theta, \tag{8}$$

$$\Phi^i_{nm} = \phi^i_{nm}/g_i k_i^2. \tag{9}$$

Here, Φ^i_{nm} is the invariant moment of the image i.

3. Multi-distortion invariant pattern recognition experiment

Twenty-six types of blood cell images, ordered as A to Z, were chosen to be the training set with intensities ranging from 0 to 255 in 64×64 pixel matrices after normalization (Fig.1). In normalization, the averaged M_{00} value of all images was taken as a constant, which was 156.06. The reference set was obtained through rotating each reference object by 15°, 30° and 45° and scaling it by 1.5 and 2 times, so as to determine the in-class variance of RHFMs. The testing set images were the rotated- (60° and 150°), scaled- (0.4 and 3 times), and intensity-changed (0.5 and 3 times) versions of the training images, without or with zero-mean additive noises σ=400 and σ=2500. Figure 2 shows the testing set of orthochromatic normoblast (image R).

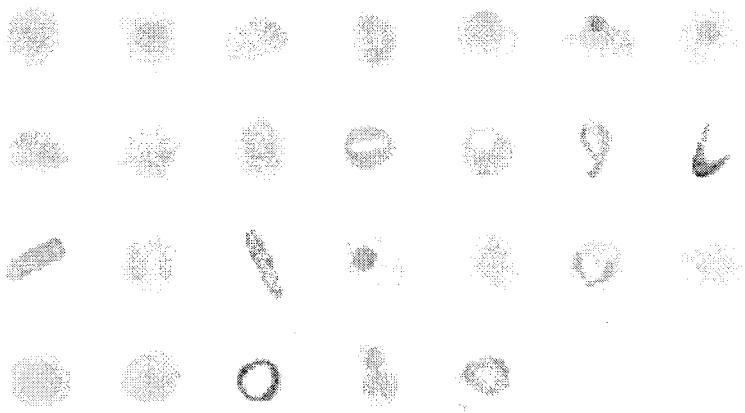


Fig.1. The training set of cell images A–Z after normalization.

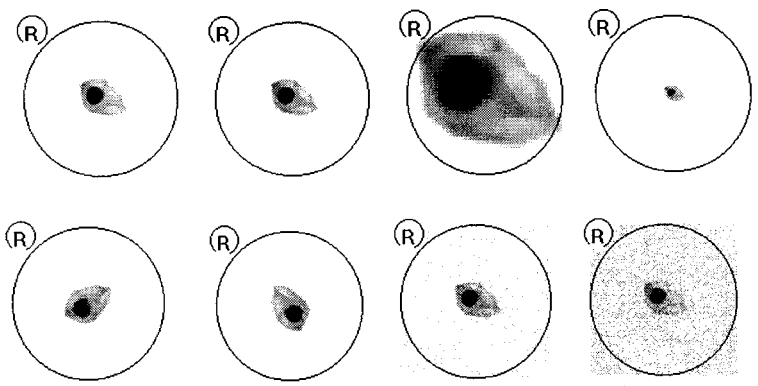


Fig.2. Testing image for the image R. From top left to bottom right: the image R has been intensity changed by 0.5 and 3 times, scaled by 3 and 0.4 times, rotated by 60° and 150°, with zero-mean additive noise of σ=400 and σ=2500.

We used 25 RHFMs with m, n=0, 1, 2, 3, 4 to describe the images, and then obtained a 25-dimensional feature space $(x_1, x_2, \cdots, x_{25})^{\mathrm{T}}$. Testing objects were classified in the feature space using the weighted minimum-mean-distance rule. The weighted distance was calculated as

$$d_i(N,M) = \left\{ \sum_{n,m=0}^{N,M} \frac{[|\Phi_{nm}| - (|\Phi_{nm}|)_i]^2}{(\sigma_{nm})_i^2} \right\}^{1/2}, \quad (10)$$

where $|\Phi_{nm}|$ is the modulus of the RHFMs of the testing object, $(|\Phi_{nm}|)_i$ are the RHFMs of the reference object of class i, and $(\sigma_{nm})_i^2$ is the in-class variance of the $(|\Phi_{nm}|)_i$. M and N are the maximum circular harmonic order and highest degree of the radial polynomials respectively.

A testing image was classified to the class i for which the distance d_i was minimum. $d_i(M,N)$ are shown in Figs.3–10 as a function of M and N with various distortions. Take the recognition of intensity-changed (3 times) image R as an example (Fig.3), the distance between it and the reference image R is the shortest, after which are reference images of images N, X, O, Z and C when M=N=4. The differences between the minimal distance and others are rather large, so it is easy to classify correctly. We can also find that in some cases, the minimal distance is not that of the test image to its reference image when lower orders are chosen. In this situation, a higher and proper order should be used. All the experimental results show that recognitions are well performed for various distorted image R with RHFMs being the feature.

The misclassification rates are zero for all testing images, except for image B with a high-level noise σ=2500. Figure 1 shows that images B and V are very similar, which causes the misclassification when high-level noise exists. More RHFMs are needed in this situation. When we used M=N=6, the above misclassification could be avoided. Images B and H with a high-level noise σ=2500 are misclassified when OFMMs are used as image feature.

When weighted minimum-mean-distance rule is used for classification, the bigger the difference between minimal distance $d_{\min}$ and sub-minimal distance $d_{\text{sub-min}}$, the stronger the distinguishing ability of the feature is. So, we define the absolute difference Δ as the subtraction of $d_{\text{sub-min}}$ and $d_{\min}$, and the relative difference λ as

$$\lambda = \frac{d_{\text{sub-min}}}{d_{\min}}. \tag{11}$$

Table 1 shows the absolute and relative differences of the image R under various distorting situations. The values in the table are rather large, indicating that the distinguishing and describing ability of RHFMs is strong. At the same time, it is highly concentrated since the correct cell image recognition is performed when only 25 features are extracted (with M=N=4). Using more RHFMs should be considered in more complicated cases.

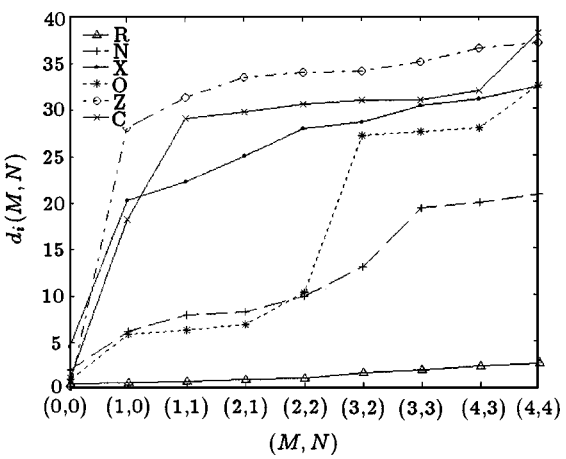


Fig.3. $d_i(M,N)$ as a function of M and N for intensity-changed image R (0.5 times).

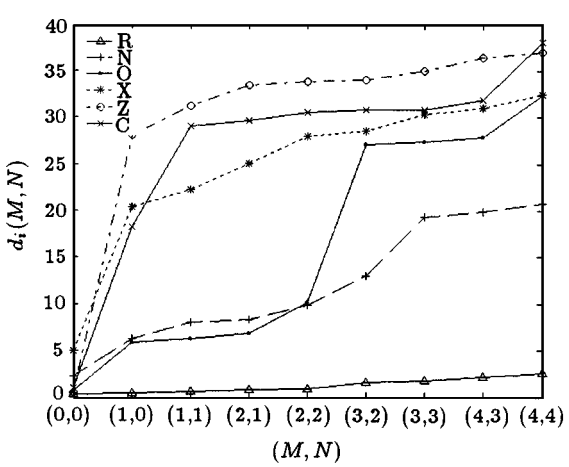


Fig.4. $d_i(M,N)$ as a function of M and N for intensity-changed image R (3 times).

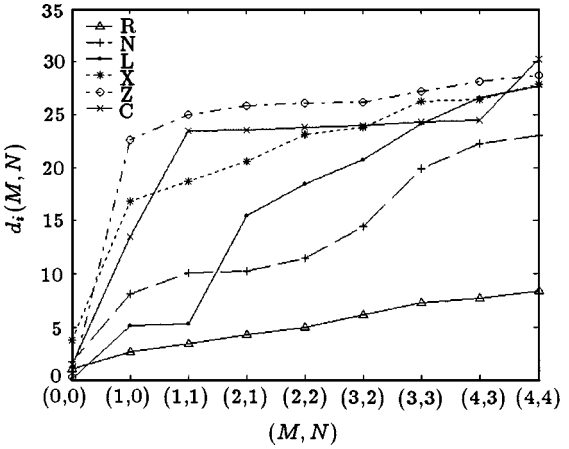


Fig.5. $d_i(M,N)$ as a function of M and N for scaled image R (0.4 times).

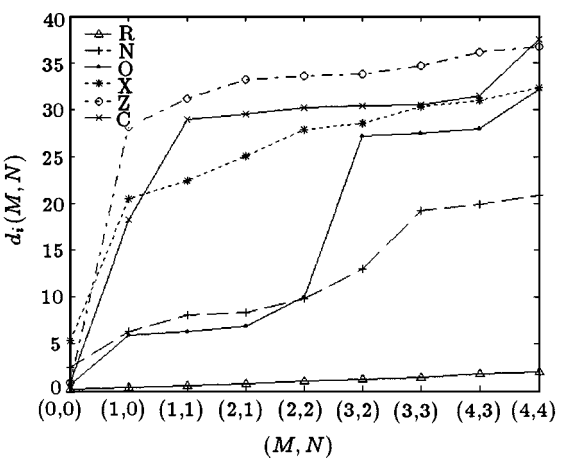


Fig.6. $d_i(M,N)$ as a function of M and N for scaled image R (3 times).

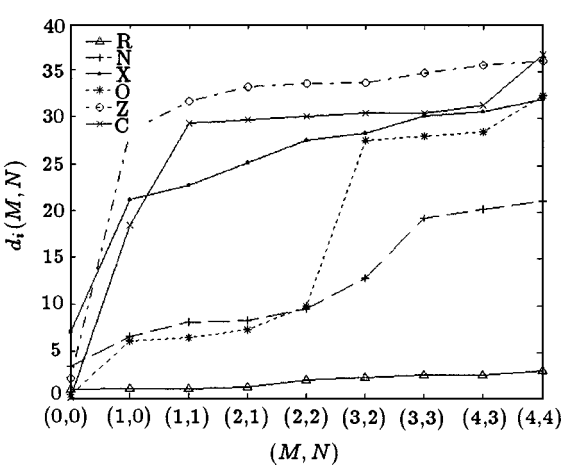


Fig.7. $d_i(M,N)$ as a function of M and N for rotated image R (60°).

Table 1. The absolute and relative differences of the testing image R.

Distortion	Distorting factor	$d_{\min}$	$d_{\text{sub-min}}$	Δ	λ
Intensity	0.5	2.60	20.79	18.19	8.00
	3	2.61	20.83	18.22	7.98
Scale	0.4	8.38	23.02	14.64	2.75
	3	2.04	20.84	18.80	10.22
Rotation	60	3.09	21.14	18.05	6.84
	150	3.34	21.05	17.71	6.30
Noise	400	3.16	21.07	17.91	6.67
	2500	9.02	21.17	12.15	2.35

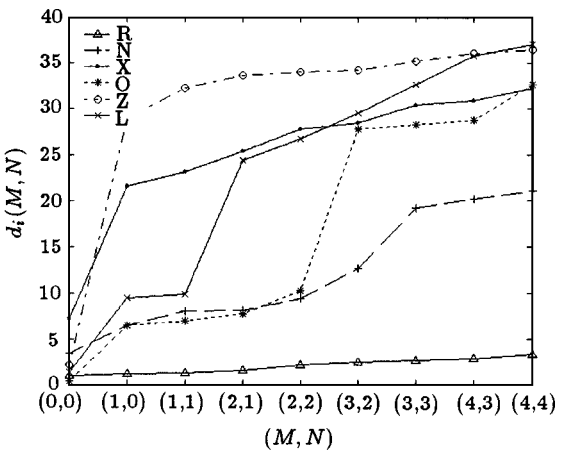


Fig.8. $d_i(M,N)$ as a function of M and N for rotated image R (150°).

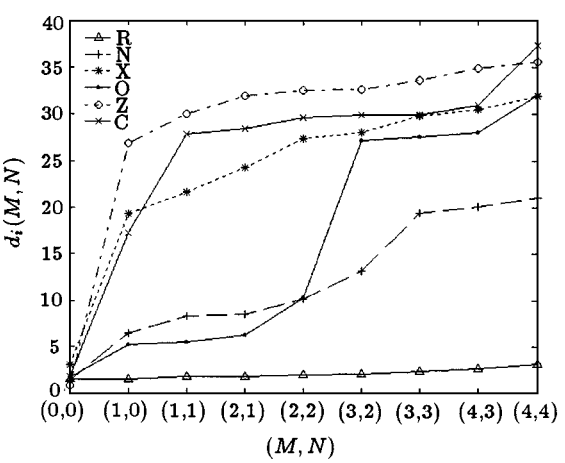


Fig.9. $d_i(M,N)$ as a function of M and N for image R added with noise (σ=400).

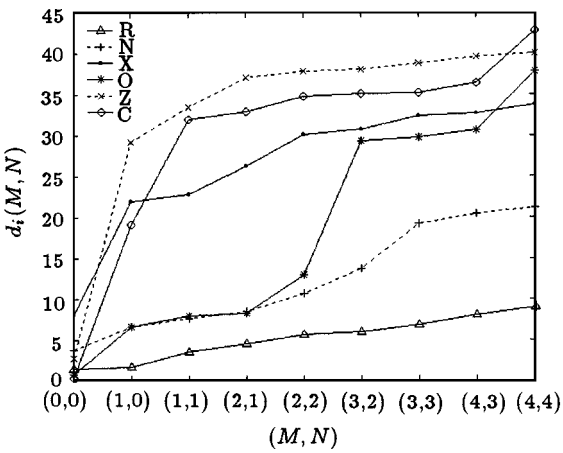


Fig.10. $d_i(M,N)$ as a function of M and N for image R added with noise (σ=2500).

4. Conclusion

We have investigated the application of RHFMs in various cell images recognition in this paper. Without any preprocessing of images, RHFMs can extract enough morphology information for accurate cell classification, which makes it easy for clinical cytological examination. Experiments show that classification of all the 208 distorted images of 26 kinds of cells can be finished within 2 min. So, as good image features, RHFMs are suitable for quick and correct cell image recognition. It will be our research focus to optimize the program, make it compatible with the clinical hardware and do some necessary case validation.

References

[1] Prokop R J and Reeves A P 1992 *CVGIP-Graph. Model. Image Proc.* **54** 438
[2] Hu M K 1962 *IEEE Trans. Inf. Theory* **IT-8** 179
[3] Teague M R 1980 *J. Opt. Soc. Am.* **70** 920
[4] Boyce J F and Hossack W J 1983 *Pattern Recogn. Lett.* **1** 451
[5] Abu-Mostafa Y S and Psaltis D 1984 *Pattern Anal. Mach. Intell.* **PAMI-6** 298
[6] Teh C H and Chin R T 1988 *Pattern Anal. Mach. Intell.* **10** 496
[7] Sheng Y L and Shen L X 1994 *J. Opt. Soc. Am.* A **11** 1748
[8] Ping Z L, Wu R G and Sheng Y L 2002 *J. Opt. Soc. Am.* A **19** 1748
[9] Ren H P *et al* 2003 *J. Opt. Soc. Am.* A **20** 631